

Effect of Discrete Suction Strips on the Stability of 3-D Boundary Layers – Direct Numerical Simulation for Boundary-Layer Flow Modelling

H. Bestek, W. Müller, M. Kloker, H. Bieler*

Institut für Aerodynamik und Gasdynamik der Universität Stuttgart, D-70550 Stuttgart

* Daimler-Benz Aerospace Airbus GmbH, D-28183 Bremen; FRG

Abstract

For the validation of physical models in boundary-layer calculations with suction the University of Stuttgart investigates together with Daimler-Benz Aerospace Airbus (DA in the following) the similarity solution due to Falkner-Skan-Cooke (FSC). For this FSC flow *strip-like suction* has been applied. In a first step several boundary-layer flows were calculated with spatial direct numerical simulations based on the 3-D Navier-Stokes equations. Linear stability theory was used to investigate the stability behaviour of these flows. In a second step boundary-layer calculations with the code HY-LISW, and stability investigations with the code COAST (both are DA in-house methods) were performed for the same setting of parameters. The results match very well with the direct-simulation data.

1 Introduction

The percentage of skin-friction related drag to the total drag is about 50 % for commercial aircrafts at cruise conditions. The combination of rather high freestream Reynolds number (for the A340 $Re_{MAC} \approx 40 \cdot 10^6$) and wing sweep angles of about $\varphi = 30^\circ$ causes turbulent flow around almost all parts of the wings. The concept of laminar flow (passive via wing shaping or hybrid with suction at the wing nose and shaping in the wing-box region) offers therefore a large technological potential in terms of drag reduction. In the frame work of the EU program BRITE/EURAM the projects ELFIN I and

II, and now HYLDA tackle problems of Hybrid Laminar Flow Control (HLFC) [1]. A 1:2 model of a modified ATTAS wing (with suction at the nose) was used in ELFIN I. The transonic wind-tunnel test in the ONERA tunnel S1MA in 1992 was successful [2].

Due to the fact that transition phenomena of a previous test in the same tunnel (ATTAS wing with NLF-glove) were calibrated with the traditional e^N -method, the prediction of boundary-layer instabilities for the suction-system design was done in the same way. This procedure, however, involves rather drastic assumptions, among which we discuss in the following the suction flow modelling in boundary-layer methods. Whereas in reality the porosity (ratio of open-to-closed surface area) at the wing nose is very small for technical reasons, i.e. suction is rather discrete, boundary-layer codes assume a 'smeared' suction-flow distribution. In addition, the effect of suction is implemented in the methods via the wall-normal boundary condition only; for mathematical reasons suction-flow effects in such codes are of parabolic nature.

Together with the University of Stuttgart [3] these approximations in industrial boundary-layer codes will be checked by comparisons with direct numerical simulations based on the 3-D Navier-Stokes equations. The model flow for this topic is an accelerated self-similar boundary-layer flow at an infinite swept wedge (FSC flow), for which the parameters have been selected according to the

above mentioned ELFIN-I HLFC experiment. The FSC model flow contains on one hand properties of a swept-wing flow (three-dimensionality!) but can on the other hand be described with just a few parameters only. Free parameters in the FSC-profiles are the wedge angle and the local sweep angle φ_e . The wedge angle $\pi\beta_H$ is related to acceleration ($\beta_H > 0$) or retardation ($\beta_H < 0$) of the boundary layer. A description of this similarity solution may be found in [4].

For this well-defined model flow Navier-Stokes simulations were performed to study the effect of one or two suction strips with varied suction-flow distribution (among these is also a ventilated case i.e. with partial outflow). Linear stability theory was applied to investigate the stability of the boundary-layer flows obtained from boundary-layer and Navier-Stokes methods. The Stuttgart group used their own spatial stability code, whereas at DA the COAST-code was applied.

2 Numerical Models

2.1 3-D Navier-Stokes Method

For direct numerical simulations (DNS) of the effects of localized suction on a spatially growing three-dimensional boundary layer a well-tested finite-difference/spectral method for the solution of the 3-D incompressible Navier-Stokes equations was employed. This code has been developed previously by Kloker [5, 6] for DNS-studies of transition in boundary layers under effect of streamwise pressure gradients. It has been applied successfully for exploring laminar-turbulent breakdown in two-dimensional [6, 7] and three-dimensional [8, 9] boundary layers, and was also employed to study the effect of single suction strips in two-dimensional boundary layers [10].

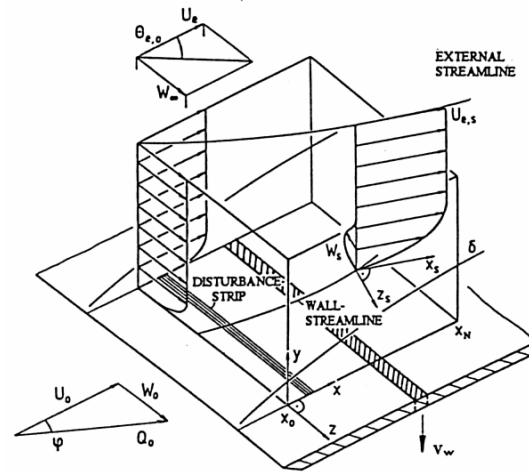


Figure 1: Integration domain for spatial DNS

The basic set-up of the numerical model is shown in Fig.1. A finite rectangular box is selected to represent a region of a three-dimensional boundary layer flow on a flat plate, with x_0 being the streamwise distance from the leading edge. In the normal y -direction, the height of the domain is chosen to cover several boundary layer thicknesses. In the spanwise z -direction, the flow is assumed to be periodic with the domain extending from $z=0$ to $z=\lambda_z$ (λ_z - fundamental spanwise wavelength). The flow quantities may also be considered in a local flow orientated coordinate system denoted by index s , which is aligned with the curved external streamline. The numerical model is based on the so-called "spatial" model, thus allowing for simulations of spatially evolving, three-dimensional disturbance waves in a growing boundary layer. Such a complete simulation is performed in two steps. First, the steady three-dimensional (formally strict: 2,5-D, $W \neq 0$, $\partial/\partial z = 0$) base flow is calculated. The base flow may be a boundary layer under combined effect of streamwise pressure gradient and local (2-D) suction through a narrow suction strip (shown schematically in Fig. 1). Then, in the second step, two- and fully three-dimensional disturbance waves with prescribed frequency and amplitude can be introduced into the domain by periodic blowing and suction through a narrow

disturbance strip (also shown in Fig. 1), and their streamwise evolution is calculated by solving the unsteady 3-D Navier-Stokes equations. All effects of non-parallel base flow, streamline curvature and nonlinearity are included in this model. However, as the simulations reported in this paper aimed at investigating the effects of localized suction on the stability of three-dimensional boundary layers, only the first of the two simulation steps was carried out, and the disturbance strip was not activated.

The numerical method is based on the three-dimensional Navier-Stokes equations for incompressible flow in vorticity-transport-velocity formulation. The vorticity components are denoted by Ω_x , Ω_y and Ω_z , and U , V and W are the velocity components in the x -, y -, and z -directions, respectively (see Fig. 1). All variables are non-dimensional, relating to the corresponding dimensional variables as

$$\begin{aligned} x &= \bar{x} / \bar{L}, \quad y = \bar{y} / \bar{L}, \quad z = \bar{z} / \bar{L}, \\ U &= \bar{U} / \bar{U}_\infty, \quad V = \bar{V} \sqrt{\text{Re}} / \bar{U}_\infty, \quad W = \bar{W} / \bar{U}_\infty. \end{aligned}$$

The Reynolds number is $\text{Re} = \bar{U}_\infty \bar{L} / \bar{\nu}$, where \bar{U}_∞ is the freestream velocity component in streamwise direction at the inflow boundary $x=x_0$. \bar{L} is a fixed reference length, and $\bar{\nu}$ is the kinematic viscosity. For the simulations presented in this paper, the Reynolds number is $\text{Re}=10^5$, where $\bar{U}_\infty = 159 \text{ m/s}$, and $L=9.434 * 10^{-3} \text{ m}$, and $\bar{\nu}=1.5 * 10^{-5} \text{ m}^2/\text{s}$.

2.1.1 Boundary Conditions

At the freestream boundary $y=y_e$, a pressure gradient is imposed by prescribing the streamwise velocity distribution $U_e(x)$ of the external flow, assuming inviscid flow. For the simulations presented in this paper, $U_e(x)$ was chosen according to a Falkner-Skan-Cooke (FSC) boundary layer ($U_e=U_0 x^m$, $m=\beta_H/(2-\beta_H)$, β_H - Hartree-Parameter). Due to the infinite swept-wing assumption the

spanwise velocity component W_e at the freestream boundary is constant along the x -axis. At the inflow boundary $x=x_0$, FSC-profiles are specified for all base-flow variables. At the outflow boundary, all equations are solved neglecting the terms with second x -derivatives. At the wall $y=0$, the velocity vector is zero, except for the suction strip; where the effect of suction through a porous strip is simulated by prescribing a normal-velocity distribution $V(x, 0)$ (see Fig. 3). In the present study, one or two suction strips with variable suction distributions are applied.

2.1.2 Numerical Method

For the numerical solution of the base-flow equations a fourth-order accurate finite-difference discretisation on a uniform grid is employed in streamwise direction and normal to the wall. The three vorticity-transport equations are solved with a partially implicit, temporally dissipative time-stepping technique to march to steady state, where the y -derivatives are treated explicitly (Forward Euler) while the x -derivatives are taken implicitly (Backward Euler). The Poisson equation for V is solved with a vectorizable, stripe pattern Gauß-Seidel-like line iteration, and the U -equation (x -derivative of the continuity equation) and the W -equation (both 2nd-order ODE BVPs) can be directly solved. This formulation optimally satisfies the continuity condition for flows with localized suction. Details of the numerical method are given by Kloker [6] and Müller [9].

2.1.3 Code Validation

For controlled transition in 2-D and 3-D boundary layers with and without streamwise pressure gradient but without suction, the numerical method was carefully validated by extensive comparisons with results from linear (spatial) stability theory, secondary instability theory and experiments [11-14]. In order to validate the code for the effect of suction through porous strips, the experiments of Reynolds and Saric [15] in a flat plate boundary layer with suction were simulated. In these experiments detailed hot-wire measurements were performed to investigate the effect of suction through discrete porous strips on the growth of Tollmien-Schlichting waves, which were introduced into the boundary layer using a vibrating ribbon. A case with one suction strip located at $Re_{\delta_1}=2300$ and a nondimensional disturbance frequency $F=\beta \bar{L}/\bar{U}_\infty \times 10^4/Re=0.25$ was chosen for comparison. In the simulation, the initial disturbance amplitude was chosen to match the amplitude at the first location of measurement in the experiment. Comparisons performed for the disturbance velocity component u' showed good agreement with the experimental results, both for the downstream amplitude evolution, and for the wall-normal amplitude distributions [10]. For a case with six suction strips, simulations were compared with theoretical results by Reed and Nayfeh [16], as reported by Bestek et al. [17]. With these thorough checks the suitability of our numerical method to simulate the effects of suction through porous strips on the stability of a 3-D boundary layer is emphasized.

2.2 Boundary Layer Methods

The LISW-boundary-layer code [18, 19] (HY-LISW is a special HLFC-oriented version) was developed to calculate steady, laminar and turbulent compressible flows. It can be applied in direct (standard) or in inverse mode. The basic equations are the momentum equations for the wall tangential directions and the total energy equation in a three-dimensional surface oriented coordinate system (x_1, x_2, x_3). These axes correspond to the flow direction, the span direction and the wall normal direction; the wall normal is perpendicular to x_1 and x_2 . In the general case the spanwise derivatives of the flow variables, but not the metric properties of the wall, will be neglected. This approach allows solutions for the locally infinite swept wing, or the solution for a section of a conical wing, which is parallel to the freestream direction. Several options are possible for the definition of the x_1 -direction with respect to leading and trailing edge; among which the option "parallel to freestream" or "normal to the leading edge" is most popular. The metric coefficients along this section may be calculated with the assumption of conical flow or may be given by the user. The calculation of the boundary-layer flow is then performed along this path or (alternatively for the purpose of comparisons) along a cut, which is implemented in the Kaups/Cebeci method [20]. For the wedge flow considered here, we have put all metric coefficients to zero and chose the option "normal to leading edge" as the integration direction. The boundary-layer integration includes a calculation of a symmetric wake flow as well.

2.2.1 Boundary Conditions

At the outer boundary (edge of the boundary-layer flow) the velocities U_{e1}, U_{e2} or the pressure distribution have to be given. The calculation starts normally at the attachment line using a given velocity distribution of the viscous stagnation flow.

However, with given so-called initial profiles it is also possible to start the integration at an arbitrary downstream position. At the wall the conditions for heat and mass transport have to be prescribed.

2.2.2 Numerical Method

The discretization in x_1 -direction is of second-order Crank-Nicolson type or of first-order upwind type (Euler Backward), with a smooth blend between these two techniques (defined by the user). The upwind technique is recommended for stability reasons, especially if abrupt changes occur in the values of the boundary conditions, which could happen for special suction distributions. The user may choose among different interpolation techniques if such suction distributions at the beginning and at the end of a chamber have to be interpolated. The upwind approach was used throughout the present investigations. Some sub-steps may be added for an improvement of the resolution. Test runs showed, that 2 to 5 sub-steps are sufficient without increasing the cpu-time noticeably.

The experience with previous cases revealed that this sub-step method combined with the Euler method produces stable and precise results, well comparable to 2nd-order results; however, no wiggles occur with the method applied. With abrupt changes in the outer boundary conditions the Crank-Nicolson method sometimes produced such instabilities.

A hermite polynomial of 4th order is used for the approximation of the derivatives in the wall-normal direction. A non-equidistant wall-normal grid may be chosen, to assure an accurate resolution in that direction. The variable grid parameter ($VGP = \delta\eta_j / \delta\eta_{j-1}$) has normally values of 1.03 to 1.06. Both momentum equations are solved via a direct solver ("implicit") at each x_1 -position. The

2×2 block tridiagonal matrices contain within an additional column the necessary boundary conditions for the inverse mode. The energy equation is solved with a standard recursion algorithm. The solution of these coupled boundary-layer equations is then gained by an iterative change of the matrix elements.

3 Model Flow

3.1 Direct Numerical Simulation

To match the DNS as closely as possible to the local flow properties of the experiment [2], an accelerated Falkner-Skan-Cooke flow with $\beta_H = 0.4$ and a local sweep angle $\varphi_e(x_0) = 35^\circ$ at the inflow boundary was chosen as base flow. The integration domain for the simulation was chosen to extend from $x_0 = 1.741$ to $x_N = 13.795$ in the streamwise x -

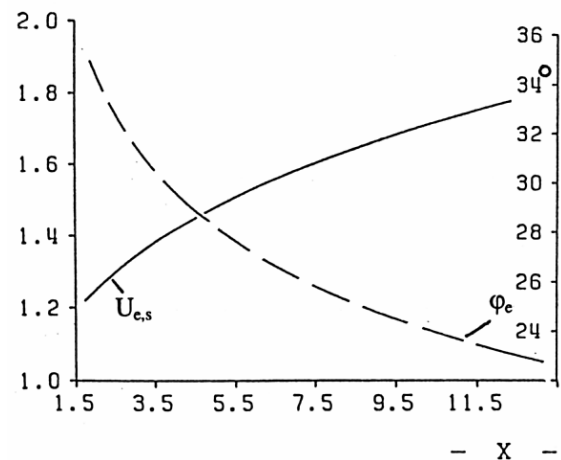


Figure 2: Boundary-layer edge velocity $U_{e,s}$ and local sweep angle φ_e of FSC model flow ($\beta_H = 0.4$)

direction, and from $y=0$ to $y_e = 17.073$ in the wall-normal y -direction, corresponding to approximately 12 boundary-layer displacement thicknesses (δ_1) at the inflow boundary; the grid size is 906×97 . The local Reynolds number at the inflow boundary $x = x_0$ is $Re_{\delta_1} = 450$, based on δ_1 in x -direction and $U_e(x_0)$ ($Re_{\delta_1} = U_e \delta_1 \sqrt{Re}$). In a local, flow-orientated coordinate system (denoted by index s , see Fig. 1) $Re_{\delta_1,s}$ is about 600. The resulting external velocity

distribution $U_{e,s}$ of the potential flow is plotted versus x in Fig. 2. The strong streamwise increase of the external velocity is accompanied by a decrease of the local sweep angle of the external streamline.

In this paper we compare the results of four different cases:

- M10: without suction (reference case)
- M11: 1 suction strip, constant suction-velocity
- M13: 1 suction strip, "ventilating"
- M22: 2 suction strips, adjusted suction-velocity distribution

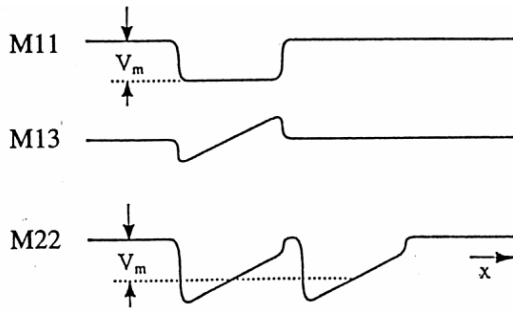


Figure 3: Sketch of suction-velocity distribution for cases M11, M13, M22

The suction velocity distributions $V_w=V(x, 0)$ used for the three suction cases are plotted schematically in Fig. 3. In agreement with the experiment [2], the mean suction velocity applied at the suction strips was $V_{w,m}=-0.298$ ($\bar{V}_{w,m}=-0.15\text{m/s}$), which is roughly 0.06% of the local potential velocity. The adjusted suction-velocity distribution, where V_w was linearly varied between (V_m-V_Δ) and (V_m+V_Δ) , $V_\Delta=0.0534$, from the upstream to the downstream end of a strip, was chosen to model the effect of the decreasing external pressure. For the "ventilating" strip we used the adjusted suction velocity distribution with zero mean $V_{w,m}=0$, resulting in weak upstream suction and weak downstream blowing. The streamwise lengths of the suction strips as well as the distance between the strips

were chosen according to the experiment [2]. The first strip was located between $4.1516 \leq x \leq 5.2305$, and the second strip was shortly downstream between $5.5102 \leq x \leq 6.589$. The local Reynolds numbers (at respective strip centers) are approximately $Re_{\delta_{1,s}}=1010$ and 1160, respectively. The strip arrangement within the integration domain allows for observing both, the upstream and the downstream effects of localized suction through discrete strips.

3.2 Boundary-Layer Calculation

For the investigation with $U_e \sim x^m$ ($m=0.25$, $c_p=1-(U/U_\infty)^2$), the sweep angle φ_∞ was chosen such that $\varphi_e(x_0)=35^\circ$. As mentioned above, the boundary-layer integration starts at the attachment line ($x=0$) with a modified Hiemenz flow ($m=1$), however, it reaches the desired similarity solution after a rather short length. We have 40 points positioned between the attachment line and x_0 , and 453 points downstream of x_0 . Thus the step size in x -direction is just twice the Δx used for the DNS. No sub-steps were necessary due to these small step sizes. The non-equidistant grid is described by $VGP=1.05$. The outer end of the integration domain is adjusted during the whole run, in order to take local changes of the boundary-layer thickness into account. For numerical reasons the value y_{max} is limited to about $7 \delta_1$.

4 Linear Stability Theory

4.1 Spatial Stability Code

The code of the University of Stuttgart considers the spatial stability problem of three-dimensional boundary-layer flows. The governing equations are the Orr-Sommerfeld and the Squire equations formulated in a body-oriented coordinate system consistent with the DNS system (see chapter 2.1). For the disturbance-velocity components u and v the normal-mode ansatz

$$[\mathbf{u}, \mathbf{v}]^T = [\mathbf{u}_k(y), \mathbf{v}_k(y)]^T \exp[i(\alpha x + \gamma z - \beta t)] + c.c.$$

is made, where α and γ are the wave numbers in x - and z -direction, β is the frequency, and $u_k(y)$ and $v_k(y)$ are the complex eigenfunctions, which give the mode structure through the boundary layer. For the spatial stability problem α is complex, and β is real. For the infinite swept-wing assumption, the cross-flow mode wave number γ is also real, so that the disturbances can only grow in x -direction. The w -velocity component is calculated from the continuity equation. The Orr-Sommerfeld-Squire problem leads to a non-trivial solution of a nonlinear eigenvalue problem with α as eigenvalue. For the numerical solution by a shooting method the 6th-order system is transformed into a system of 6 1st-order ODEs. No-slip conditions at the wall and an exponential decay of disturbances in the freestream are used for the boundary conditions (see [21] for details). The 6 1st-order ODEs are integrated with a classical Runge-Kutta scheme of 4th-order accuracy, starting with initial values outside of the boundary layer. An estimate is needed for α , which should lie close to the converged eigenvalue. In order to suppress the growth of unphysical solutions, all solution vectors are normalized after each complete Runge-Kutta step following the Gram-Schmidt orthonormalization technique. The estimate for α is iteratively improved up to a convergence of the solution to the boundary conditions at the wall.

4.2 DA Stability Code COAST

The DA-code COAST considers the stability problem of compressible boundary-layer flows [22, 23]. The basic flow contained in the eigenvalue equations is - in contrast to the simulation approach (see chapter 4.1) - a solution of the boundary-layer equations. The disturbance equations are formulated as a system of 4 ODEs of 2nd order and 1 ODE of 1st order. A similar approach may be found in [24]. Using the temporal approach we impose real wave numbers α and γ . The stability equations form a generalized eigenvalue problem for the complex frequency β . This was transformed at DA into a simple eigenvalue problem. The wall-normal coordinate z is transformed via an algebraic stretching function and the resulting system of differential equations is then solved with a central-difference scheme of 2nd order. The local spatial amplification follows from an application of the Gaster transformation [25]. The code contains several integration strategies for the N-factors, among which the so-called NTS-NCF-model is widely applied at DA (TS for Tollmien-Schlichting modes and CF for cross-flow modes) :

- stationary modes (0 Hz modes) of constant wave length are considered for the NCF factors, based on the appearance of stationary cross-flow vortices in transition experiments with cross-flow dominated transition
- the NTS -factors are calculated with the use of travelling modes (of higher frequency within the whole spectrum), which run parallel to the local potential streamline (fixed frequency approach)
- there is the additional possibility to investigate the maximum amplification for each single fixed-frequency mode, which results in so-called N-factors of the envelope method.

The direction of the group velocity dictates the integration path for all strategies, because this group velocity follows the direction of some energy transport. However, we consider here the strategy of constant spanwise wave number, in order to compare the results with the data of the spatial approach.

5 Results

5.1 Comparisons for the Shape Factor

For self-similar boundary layers, such as the FSC flow considered here, the shape factor H_{12} based on U (in x -direction) is constant. This is captured by the simulation (Fig. 4a) as well as by the boundary-layer calculation (Fig. 4b) for the reference case M10 without suction, as indicated by the straight lines in Figs. 4a, b. For the suction cases (M11, M22) the shape factor H_{12} is distinctly decreased at the suction strip locations. For the second suction strip the minimum of H_{12} is only slightly lower than for the first strip. With respect to the effect of the suction-velocity distribution, only minor differences are observed for the shape factor distribution at the first strip, when comparing case M11 (constant distribution) with case M22 (adjusted distribution). Downstream of the suction strip(s) the shape factor increases again, up to values even larger than for the reference case, and is then slowly decaying to approach the value of the reference case asymptotically, indicating a far-reaching downstream influence on the base flow. The overshoot of H_{12} downstream of the suction area indicates a locally more unstable U -profile than without suction. This phenomenon is not known for two-dimensional boundary-layer flows, where the shape factor was found to approach the reference value for no suction asymptotically from below, see [10]. For the ventilating strip (case M13) the shape factor changes only locally above the strip.

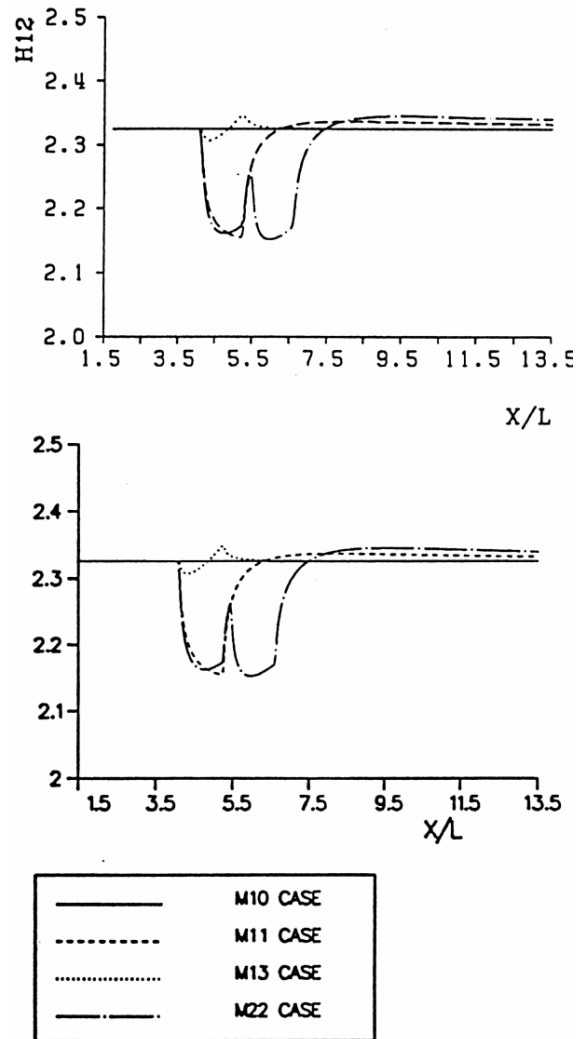


Figure 4: Evolution of shape factor H_{12} for FSC-flow with different suction distributions (cf. Fig. 3)
 a) Navier-Stokes simulation (Univ. Stuttgart)
 b) boundary-layer calculation (DA)

When comparing the shape-factor distributions obtained from the simulations (Fig.4a) with those obtained from the boundary-layer calculations (Fig. 4b), very good quantitative agreement can be observed for all cases. This is caused by the fact that (at least for the suction cases considered here) a suction *strip* in accelerated three-dimensional boundary layers exerts virtually no upstream influence, as can be seen from Fig. 4a. Hence the assumption of neglectable upstream influence inherent in boundary-layer methods seems well justified in this case.

Very good agreement between the results of the two different numerical models is also observed for the velocity profiles of U_s and W_s . In Fig. 5, velocity profiles obtained from the boundary-layer calculations for the cases M10, M11 and M22 are plotted at $x=6.589$ (at the downstream end of the second suction strip). The stabilizing effect of one

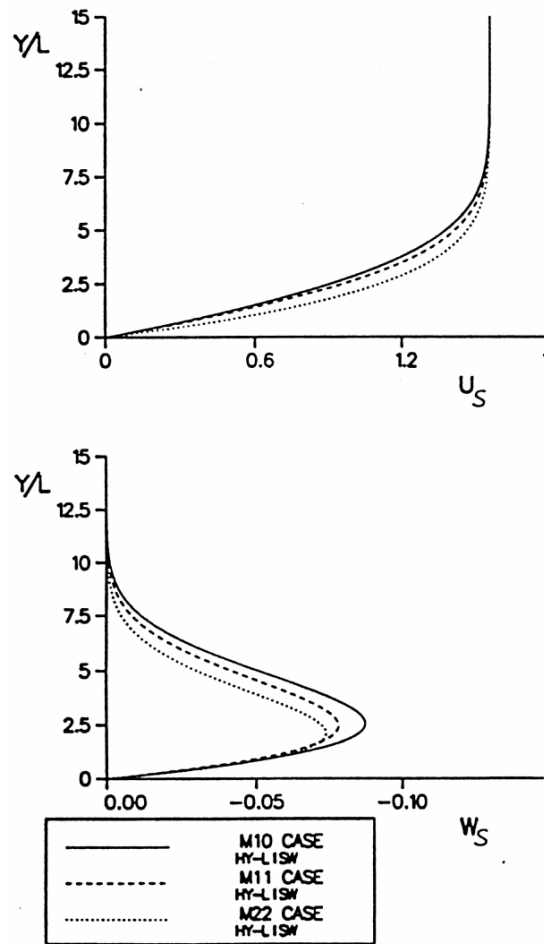


Figure 5: Velocity profiles U_s and W_s for FSC-flow with different suction distributions (cf. Fig. 3) at $x=6.589$ (DA)

and two suction strips on the velocity profiles is clearly visible: the U_s -profile for the streamwise velocity component is filled up close to the wall, while for the cross flow velocity component the maximum of the W_s -profile is reduced by each suction strip, and its y -position is shifted towards the wall.

The effect of suction on the cross flow is illustrated in Fig. 6, where the maximum $W_{s,max}$ of the cross flow velocity component is plotted versus x for the four cases. The curve for case M11 shows that $W_{s,max}$ is effectively reduced by localized suction through a single strip. The effects of two suction strips sum up, as is seen for case M22. For the ventilating strip (case M13), a very small increase of $W_{s,max}$ can be observed downstream of $x \approx 7.0$. This effect is really insignificant compared to the effects for case M11, however, it confirms the tendency of destabilization, which is expected for the ventilating strip.

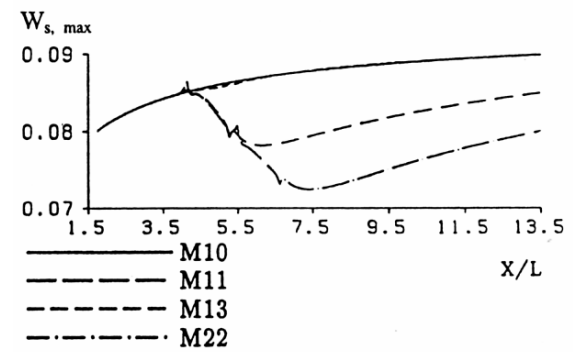


Figure 6: Streamwise evolution of maximum cross flow velocity $W_{s,max}$ (Univ. Stuttgart)

5.2 Stability Characteristics

The local stability characteristics of the base flows for the four cases were determined from linear (spatial) stability calculations. In the framework of this study stationary disturbances (e.g. so-called 0-Hz-modes or cross-flow vortices) were considered only. The stability diagrams for these modes, resulting from stability calculations for the base-flow profiles within the entire integration domain are shown in Figs. 7a to 7c for the cases M10, M11 and M22. Here, lines of constant spatial amplification rate α_i are plotted in the γ - x -plane,

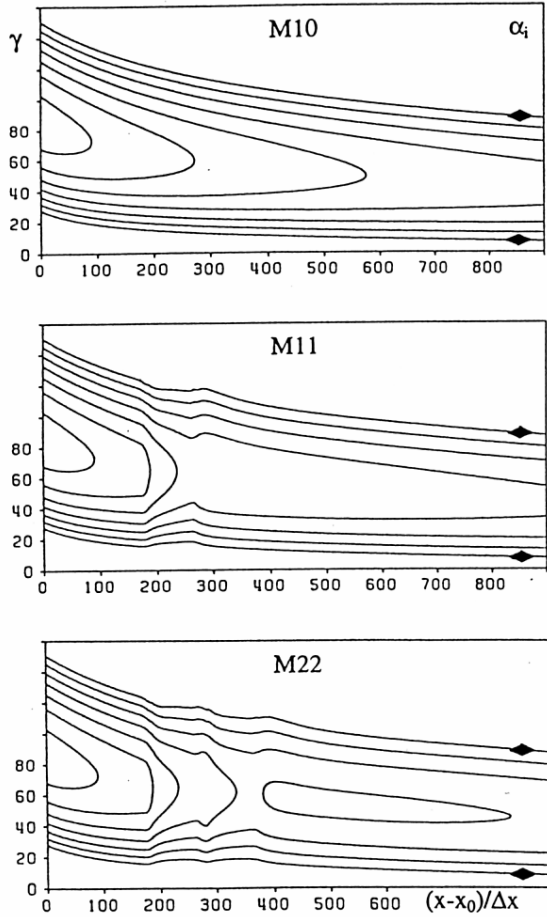


Figure 7: Contours of constant amplification rates (symbols: neutral) for 0-Hz modes for FSC-flow with different suction distributions (cf. Fig. 3, M10: reference case)

where γ is the spanwise wave number of the cross-flow vortices. The outermost upper and lower curves are the so-called neutral curves for zero amplification rate ($\alpha_i=0$), where the cross-flow vortices show a neutral amplitude behavior. Thus the neutral curves separate the unstable (inner) domain from the stable (outer) domain. Within the unstable domain equidistant lines of constant α_i are plotted with an increase by $\Delta\alpha_i=0.2$ between two lines.

The basic stability characteristics of the FSC-flow are now discussed briefly for the reference case (Fig. 7a). With increasing Reynolds number the

band width of unstable spanwise wave numbers is considerably contracted, while the maximum amplification rate is decreased. The band width of unstable cross-flow modes is therefore rather narrow in downstream direction. When comparing the stability diagram for case M11 (Fig. 7b) with Fig. 7a, the expected stabilizing effect of the suction strip becomes apparent in lower amplification rates for the most unstable cross-flow wave numbers γ . However, shortly downstream of the strip, the band of amplified cross-flow modes is shifted to higher wave numbers. This phenomenon is preserved up to the end of the integration domain.

In order to describe the transition process the integral rather than the local amplification rates are of importance. A well-known measure for this topic is the N-factor, which might be calculated from the local amplification rates α_i as $N=\ln(A/A_0)=-\int\alpha_i dx$. The integration using the temporal code COAST applies the Gaster-transformation and the integration path follows the path of the group velocity of the corresponding mode. Usually the integration starts at the neutral point of each mode. But in our case most of these points are upstream of the integration box. Therefore, we started the integration at x_0 , which is sufficient to demonstrate the effect of different suction configurations. A comparison of N-factors from boundary-layer stability analysis and from the simulation is shown in Figs. 8-10 (for cases M10 and M22) for fixed cross-flow wave numbers in the region $x_0 \leq x \leq 10.5$. The largest N-factors were reached by the modes $40 \leq \gamma \leq 80$. The envelope coincides almost with the $\gamma=60$ curve and represents therefore the largest N-factor variation. For the reference case (Fig. 8) a N-factor of about 8 is reached within the considered integration region, which corresponds to an absolute amplitude (A/A_0) increase by a factor of 2981.

Due to suction by two strips (M22) the maximum N-factor drops to about 6.8 at $x=10.5$ (Figs. 9, 10). If one follows the N-factors of the envelopes, which are shown in Fig. 11 for all four cases, the effect of a single and two suction strips onto the N-factors appear obvious. Keeping in mind, that the suction rate applied at the strip is rather weak a considerable reduction of the N-factor is achieved within the considered x-region. For the ventilating case M13 no deviations from the reference case M10 can be observed in Fig. 11. Finally, a comparison of Fig. 9 and Fig. 10 for case M22 reveals a good agreement of the COAST results (based on the boundary-layer profiles) with the spatial stability results (based on the DNS base flow).

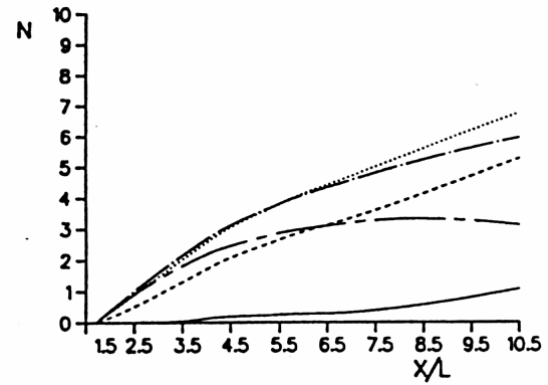


Figure 9: N-factors of FSC-flow with suction (case M22, for caption see Fig. 8)

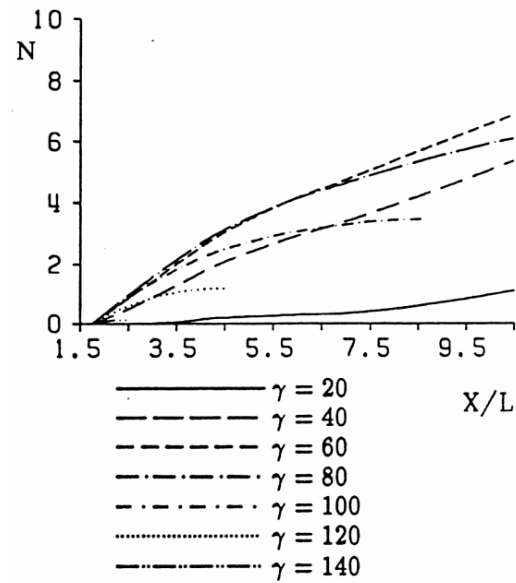


Figure 10: Same as Fig. 9, now with Univ. Stuttgart method

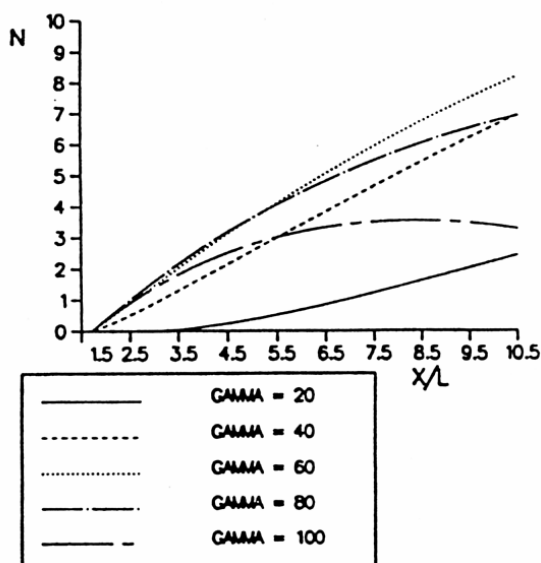


Figure 8: N-factors of FSC reference flow (case M10) for different spanwise wave numbers γ (DA)

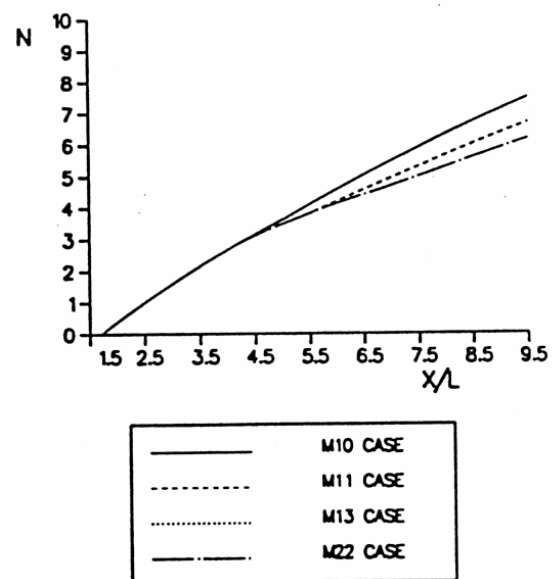


Figure 11: Envelopes of N-factors for all cases, cf. Fig. 3 (DA)

6 Remarks and Outlook

Accurate transition prediction is an important aspect for the design of HLFC wings. The application of traditional e^N -methods requires the modelling of the suction flow in boundary-layer methods. The overall efficacy of a HLFC suction system may be examined in wind-tunnel tests; however, the great number of parameters affecting the transitional evolution does not allow to examine the different modelling assumptions.

In a combined effort by DA and the University of Stuttgart spatial DNS are employed to investigate the flow details for suction through porous panels in order to check the suction-flow modelling in boundary-layer methods. In the first part of this project reported in this paper, the effects of *spanwise suction strips* on a 3-D boundary layer modelled by a suction-flow velocity distribution were investigated. The model flow chosen for this project is the well-defined Falkner-Skan-Cooke flow, with parameters selected according to the ELFIN-I HLFC-experiment. Results from DNS-studies for one or two suction strips, where the suction flow was adjusted to the experiment, showed very good quantitative agreement with corresponding boundary-layer calculations. This agreement is most likely due to the *weak suction rate* considered here, causing no non-negligible upstream influence on the 3-D boundary layer with its favourable pressure gradient.

The second part of this project is concerned with detailed investigations of suction through *arrays of discrete holes* in a 3-D boundary layer. As shown in Fig. 12, where the negative v -velocity at the wall is plotted in perspective view, suction through a spanwise array of holes can be represented in the DNS-code (with its spanwise spectral ansatz) by superposition of a large number (here: 20) of steady

spanwise modes with equal z -phase and amplitude, varied over the disturbance-input region in x .

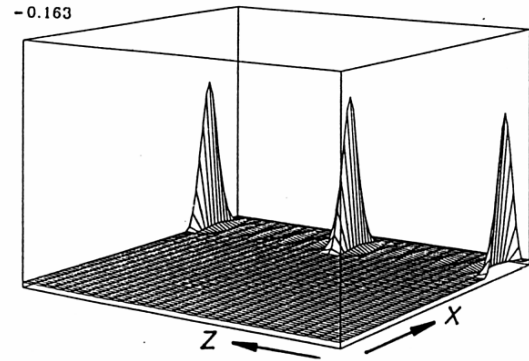


Figure 12: Perspective view of effective wall-normal velocity in DNS on plate surface for suction with array of discrete holes

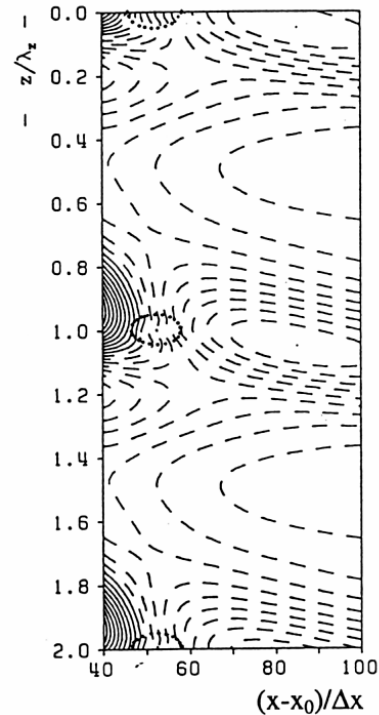


Figure 13: Contours of spanwise vorticity (ω_z) disturbance at the wall for suction with array of discrete holes (dotted regions) in 3-D FSC-flow

Preliminary results of test calculations already indicate a complicated flow structure with upstream influence, as can be seen from the ω_z wall-vorticity distribution (Fig. 13), where the suction holes are located around $z/\lambda_z=0, 1, 2$ and $x/\Delta x=52$. From these investigations, we expect a detailed insight

into the flow phenomena in a 3-D boundary layer under the effects of localized strong suction through micro-holes.

7 References

- [1] Bieler, H.: Hybrid Laminarisierung für Verkehrsflugzeuge - Vorbereitung eines Windkanalversuches mit einem modifizierten ATTAS-Handschuh, *Proc. DGLR-Jahrestagung 1991 Berlin, DGLR-Jahrbuch 1991*, Vol. I, pp. 751-758 (1991).
- [2] Henke, R., Garcon, F., Bieler, H., Preist, J.: Hybrid Laminar Flow Control: The ELFIN Wind Tunnel Test Campaign, 2. *Aerodays of the EU*; Paper in Session 4a; Naples, Oct.4-5 (1993).
- [3] Müller, W., Bestek, H.: *Räumliche Navier-Stokes-Simulationen zur Untersuchung einer 3-D-Grenzschichtströmung mit lokaler Absaugung*, Abschlußbericht zum Forschungsauftrag der Deutschen Aerospace Airbus GmbH. Universität Stuttgart, Institut für Aerodynamik und Gasdynamik (1993).
- [4] Schlichting, H.: *Boundary-Layer Theory*. McGraw Hill, New York (1977).
- [5] Kloker, M., Konzelmann, U., Fasel, H.: Outflow Boundary Conditions for Spatial Navier-Stokes Simulations of Transition Boundary Layers, *AIAA-J. 31*, pp. 620-628 (1993).
- [6] Kloker, M.: *Direkte numerische Simulation des laminar-turbulenten Strömungsumschlages in einer stark verzögerten Grenzschicht*, Dissertation, Universität Stuttgart (1993).
- [7] Kloker, M., Fasel, H.: Direct Numerical Simulation of Boundary-Layer Transition with Strong Adverse Pressure Gradient. *Proc. 4th IUTAM-Symposium on Laminar-Turbulent Transition*, Sendai, Japan, 1994 (R. Kobayashi, ed.), pp. 481-488, Springer, Berlin (1995)
- [8] Müller, W., Bestek, H., Fasel, H.: Spatial Direct Numerical Simulation of Transition in a Three-Dimensional Boundary Layer. *Proc. 4th IUTAM-Symposium on Laminar-Turbulent Transition*, Sendai, Japan, 1994 (R. Kobayashi, ed.), pp. 397-404, Springer, Berlin (1995)
- [9] Müller, W.: *Numerische Untersuchung räumlicher Umschlagvorgänge in dreidimensionalen Grenzschichtströmungen*, Dissertation, Universität Stuttgart (1995).
- [10] Müller, W., Kloker, M., Bestek, H.: Numerical Investigation of the Effect of Local Suction on Transition in a Boundary Layer with Adverse Pressure Gradient, *Proc. First European Forum on Laminar Flow Technology*, DGLR-AAAF-RAeS, Hamburg, 1992, DGLR-Bericht 92-06, pp. 59-66 (1992).
- [11] Fasel, H., Rist, U., Konzelmann, U.: Numerical Investigation of the Three-Dimensional Development in Boundary-Layer Transition, *AIAA-J. 28*, pp. 29-37, 1990.
- [12] Rist, U., Fasel, H.: Direct Numerical Simulation of Controlled Transition in a Flat-Plate Boundary Layer, *J. Fluid Mech. 298*, pp. 211-248 (1995).
- [13] Kloker, M., Fasel, H.: Numerical Simulation of Two- and Three-Dimensional Instability Waves in Two-Dimensional Boundary Layers with Streamwise Pressure Gradient, *Proc. 3rd IUTAM-Symposium on Laminar-Turbulent Transition*, Toulouse, France, 1989 (R. Michel, D. Arnal, eds.), pp. 681-686, Springer, Berlin (1990)
- [14] Müller, W., Bestek, H., Fasel, H.: Numerical Simulation of the Spatial Disturbance Development in Transitional Boundary Layers along a Swept Plate, *Near-Wall Turbulent Flows* (R.M.C. So, C.G. Speziale, B.E. Launder, eds.), pp. 869-878, Elsevier Science Publishers B.V. (1993).

- [15] Reynolds, G.A., Saric, W.S.: Experiments on the Stability of the Flat-Plate Boundary Layer with Suction, *AIAA-J.* 24, pp. 202-207 (1986).
- [16] Reed, H.L., Nayfeh, A.H.: Numerical-Perturbation Technique for Stability of Flat-Plate Boundary Layers with Suction, *AIAA-J.* 24, pp. 208-214 (1986).
- [17] Bestek, H., Konzelmann, U., Fasel, H.: Numerische Untersuchung zum Einfluß lokaler Absaugung auf die Stabilität der Plattengrenzschichtströmung, *ZAMM* 69, T593-T596 (1989).
- [18] Elsholz, E.: *Ein inverses LISW-Grenzschicht-Differenzenverfahren.* MBB-Bericht TE 2-1681, Nov. 1988.
- [19] Elsholz, E.: *LISW-Grenzschichtdifferenzenverfahren für Anwendungen in der Laminartechnologie.* DA-Bericht EF-1894 (1992).
- [20] Kaups, K., Cebeci, T.: Compressible Laminar Boundary Layers with Suction on Swept and Tapered Wings, *J. Aircraft* 14, pp. 661-667 (1977).
- [21] Müller, W., Bieler, H., Kloker, M., Bestek, H.: Direkte räumliche Simulation von dreidimensionalen Grenzschichten mit Absaugung zur Überprüfung der Modellbildung in Grenzschichtverfahren, *Proc. DGLR-Jahrestagung 1994*, Erlangen, *DGLR-Jahrbuch 1994*, Vol. II, pp. 991-1000 (1994).
- [22] Schrauf, G.: *COAST - A compressible stability code. User's guide and tutorial.* MBB-Report TE 2-1751, December 1989, and TLF-Ergebnisbericht Nr. 9, Januar 1990.
- [23] Schrauf, G.: Algorithm 696: An inverse Rayleigh iteration for complex band matrices. *ACM Transactions on Mathematical Software* 17, pp. 335-340 (1991).
- [24] Malik, M.R., Orszag, S.A.: Efficient Computation of the Stability of Three-Dimensional Compressible Boundary Layers, *AIAA-Paper 81-1277* (1981).
- [25] Gaster, M.: A note on the relation between temporally-increasing and spatially-increasing disturbances in hydrodynamic stability, *J. Fluid Mech.* 14, pp. 222-224 (1962)